processes

MDPI

Article

Optimization Design of an Intermediate Fluid Thermoelectric Generator for Exhaust Waste Heat Recovery

Wei Zhang [1], Wenjie Li [2], Shuqian Li [3], Liyao Xie [2], Minghui Ge [2,*] and Yulong Zhao [2,*]

[1] College of Mechanical and Electrical Engineering, Shihezi University, Shihezi 832003, China; lihankong357@163.com
[2] Hebei Key Laboratory of Thermal Science and Energy Clean Utilization, Hebei University of Technology, Tianjin 300401, China; 18832006409@163.com (W.L.); xieliyao@hebut.edu.cn (L.X.)
[3] Hebei Technology Innovation Center of Phase Change Thermal Management of Data Center, Hebei University of Water Resources and Electric Engineering, Cangzhou 061001, China; lsctcc@163.com
* Correspondence: geminghui@hebut.edu.cn (M.G.); zhaoyulong@hebut.edu.cn (Y.Z.)

Abstract: The intermediate fluid thermoelectric generator (IFTEG) represents a novel approach to power generation, predicated upon the principles of gravity heat pipe technology. Its key advantages include high-power output and a compact module area. The generator's performance, however, is influenced by the variable exhaust parameters typical of automobile operation, which presents a significant challenge in the design process. The present study establishes a mathematical model to optimize the design of the IFTEG. Our findings suggest that the optimal module area sees substantial growth with an increase in both the exhaust heat exchanger area and the exhaust flow rate. Interestingly, the optimal module area appears to demonstrate a low sensitivity to changes in exhaust temperature. To address the challenge of determining the optimal module area, this study introduces the concept of peak power deviation. This method posits that any deviation from the optimal module area results in an equivalent power deviation. For instance, with an exhaust heat exchanger area of 1.6 m^2, the minimum peak power deviation is 27.5%, corresponding to a design module area of 0.124 m^2. As such, the actual output power's deviation from the maximum achievable output power will not exceed 27.5% for any given set of exhaust parameters. This study extends its findings to delineate the relationship between the optimal design module area and the exhaust heat exchanger area. These insights could serve as a useful guide for the design of future power generators.

Keywords: thermoelectric generator; intermediate fluid; power deviation; optimization

check for updates

Citation: Zhang, W.; Li, W.; Li, S.; Xie, L.; Ge, M.; Zhao, Y. Optimization Design of an Intermediate Fluid Thermoelectric Generator for Exhaust Waste Heat Recovery. *Processes* **2023**, *11*, 1853. https://doi.org/10.3390/pr11061853

Academic Editor: Farooq Sher

Received: 18 May 2023
Revised: 15 June 2023
Accepted: 16 June 2023
Published: 20 June 2023

Copyright: © 2023 by the authors. Licensee MDPI, Basel, Switzerland. This article is an open access article distributed under the terms and conditions of the Creative Commons Attribution (CC BY) license (https://creativecommons.org/licenses/by/4.0/).

1. Introduction

The escalating energy scarcity has catalyzed the refinement of extant energy utilization and the investigation of novel energy resources [1]. As a prominent sector of energy consumption, environmental pollution engendered by the swift expansion of the transportation industry is progressively worsening. The fuel efficiency of internal combustion engines remains suboptimal, with an excess of 30% of fuel energy dispelled as exhaust [2]. The recovery and utilization of this fraction of energy would undeniably yield substantial energy conservation and emission reduction benefits.

Technologies such as the organic rankine cycle system [3], turbomachinery [4], and the thermoelectric generator (TEG) [5] have demonstrated the capacity to convert heat energy from the automobile exhaust into usable, high-quality energy. These technologies have garnered considerable attention in recent years. The exhaust thermoelectric generator (ETEG) employs the Seebeck effect [6] to convert waste heat from the exhaust directly into electricity [7]. This electricity can then be used to power auxiliary equipment in the vehicle [8]. However, the efficiency deficit of ETEGs remains a significant barrier to their broader application. An ETEG is composed of an exhaust heat exchanger (EHE), a heat sink, and thermoelectric modules (TEMs). The efficiency of the ETEG hinges not only on the

properties of the thermoelectric materials used but also on the heat transfer capacity of the EHE. The heat transfer resistance between the exhaust and the EHE surface results in a TEM hot-end temperature that is significantly lower than the exhaust temperature [9]. Given that the temperature gradient between the hot and cold ends of the TEM is proportional to its conversion efficiency, employing an EHE with superior heat transfer performance can substantially elevate the hot-end temperature. Consequently, this enhances the thermoelectric conversion efficiency of the ETEG.

Enhancement of the heat transfer capacity in an EHE is commonly achieved through the installation of fins within the exhaust channel. Lu et al. strategically arranged non-uniform fins inside an EHE, resulting in a 177.4% increase in net output power, with an air Reynolds number ranging from 3000 to 6400 and an inlet temperature between 523 and 553 K [10]. Similarly, Ma et al. incorporated four sets of fins, angled at 45° to the airflow direction, in the exhaust channel, thereby augmenting the convective heat transfer of the exhaust [11]. Chen et al. utilized conventional plate fins and square pin fins in an EHE flow channel, noting that an optimal count of 78 square pin fins led to an ETEG output power of 24.14%, superior to the plate fin EHE [12]. Marvão et al. advocated for minimal fin thickness in an EHE to maximize the net output power increase of the ETEG [13]. In a separate study, Luo et al. constructed a multiphysics coupling model of an ETEG, achieving an output power and conversion efficiency of 38.07 W and 1.53%, respectively, at a vehicle speed of 120 km/h [14]. Liu et al. explored the impact of fin parameters on the thermoelectric properties and pressure drop of an ETEG [15]. By optimizing these parameters, they were able to elevate the average temperature of the EHE while simultaneously reducing flow resistance by 20%. Similarly, Fernández-Yañez et al. [16] discovered that optimal ETEG performance was achieved when the baffle arrangement angle in the exhaust channel was in alignment with the exhaust inlet direction, a finding corroborated by other studies [17]. Su et al. divided an EHE into three sections and introduced a folding plate-reinforced structure [18]. Their research aimed to find the optimal heat exchanger structure by examining the length and thickness of the folded plate in relation to surface temperature and thermal uniformity. However, the optimized structure significantly impaired the efficiency of the internal combustion engine due to the substantial back pressure it generated. Karana et al. employed an EHE equipped with a twisted strip to attain maximum output power at an intercept ratio of 8, a torque ratio of 4, and an inclination angle of 60° [19]. Lesage reported that flat inserts with notches outperformed spiral inserts in terms of heat transfer, resulting in an over 50% increase in net output power compared to smooth channels [20]. Wang et al. [21] advocated for enhancing exhaust heat transfer with a circular sunken surface, implementing this in an ETEG for the waste heat recovery of an off-road vehicle [22]. At a speed of 125 km/h, the system's net power reached 133.46 W, marking an increase of 173.6% compared to the ETEG with a finned EHE.

Porous structures have been employed as a means of enhancing the thermoelectric performance of the ETEG due to their proficient heat transfer capacities. Choi et al. integrated a porous plate with a porosity of 0.416 into an EHE, leading to a conversion efficiency of 2.83% in the ETEG, a value that is 10.1% higher compared to that achieved with a smooth exhaust channel [23]. Similarly, Negash et al. conducted a study on the influence of the porosity and location of the porous plate on the thermoelectric performance of ETEG systems, discovering that variations in porosity induced changes in the optimal position of the porous plate [24]. In a separate investigation, Li et al. filled an EHE with metal foam, thereby quadrupling the convective heat transfer coefficient [25]. However, this also resulted in a significant amplification of the exhaust duct resistance. Bai et al. noted that the incorporation of metal foam not only boosted the ETEG output power by 170% but also curtailed the average noise level by 16.6 dB [26]. Other researchers have proposed the insertion of vertebral bodies into the EHE to augment the convective heat transfer of the exhaust. Musial et al. managed to elevate the efficiency of an ETEG by 25% by incorporating a cone into the EHE [27]. Shu et al. added an air deflector to a hexagonal EHE and coupled TEMs with diverse thermoelectric materials to accommodate

the attenuation of exhaust temperature, which resulted in an output power of 78.9 W, a 30% improvement over the use of a single thermoelectric material [28]. Shen et al. found that the inclusion of hollow cylinders could effectively enhance the performance of an ETEG, provided that the EHE diameter is equal to or greater than 75 mm [29].

During the operation of a vehicle, it is noted that exhaust parameters tend to fluctuate [30], a factor that directly influences the performance of the ETEG. Aranguren et al. discovered that an ETEG's output power reached its peak of 24.59 W at an exhaust temperature and flow rate of 560 °C and 170 kg/h, respectively [31]. Diminishing the exhaust temperature to 525 °C led to an 11% reduction in power generation, while a decrement in the flow rate to 133 kg/h resulted in a 6% decline in power generation. Garud et al. conducted a study on the impacts of air inlet temperature on an ETEG's power generation performance. The ETEG's efficiency reached 1.88% at an inlet temperature of 600 °C, a stark contrast to the efficiency of 1.31% that was recorded at 500 °C [32]. Additionally, He et al. observed a decrease in the performance of a TEM due to a gradual reduction in exhaust temperature. The researchers found that there was an optimal TEM area for maximizing output power, and that this optimal TEM area was influenced by the exhaust parameters [33].

The authors have previously presented work on the intermediate fluid thermoelectric generator (IFTEG) [34]. This system employs the gas–liquid phase transition of an intermediate fluid (IFD) to facilitate exhaust heat transfer. It offers the substantial increase in output power of 32.6% while concurrently reducing the TEM area, leading to significant economic benefits. However, given the variability in exhaust parameters, ensuring efficient generator operation under all working conditions presents a design challenge. Therefore, the present study commences by examining the impact of exhaust parameters on the optimal structural parameters of the system. The pivotal design parameters of the IFTEG, along with their influencing factors, are scrutinized using the minimum deviation method. This method targets the limit output power while factoring in the fluctuation of exhaust parameters. The insights derived from this analysis can inform and guide the optimal design of the IFTEG system.

2. Intermediate Fluid Thermoelectric Generator

Figure 1 depicts the structure of the IFTEG, a novel type of thermoelectric generator grounded in the principles of the gravity heat pipe. The IFTEG primarily comprises an EHE, a phase change cavity, TEMs, and a cooling water heat exchanger [34]. The phase change cavity is filled with an IFD and is maintained in a sealed state. The EHE tube is submerged in the IFD, functioning analogously to the boiling section of a heat pipe. The apex of the cavity, designed as a vertical square cavity to enable the flow of condensed fluid back to the liquid pool, represents the condensing section of the heat pipe. The TEM is positioned between the condensing section of the cavity and the cooling water heat exchanger, which respectively function as the hot and cold ends of the module. When the exhaust enters the EHE tube, the high-temperature exhaust induces the IFD within the phase-change cavity to vaporize. This vapor then dissipates heat in the condensing section, leading to condensate formation, which flows back to the liquid pool under gravity. The heat from condensation is introduced into the TEM to generate electrical energy, with any residual heat being removed with the cooling water heat exchanger.

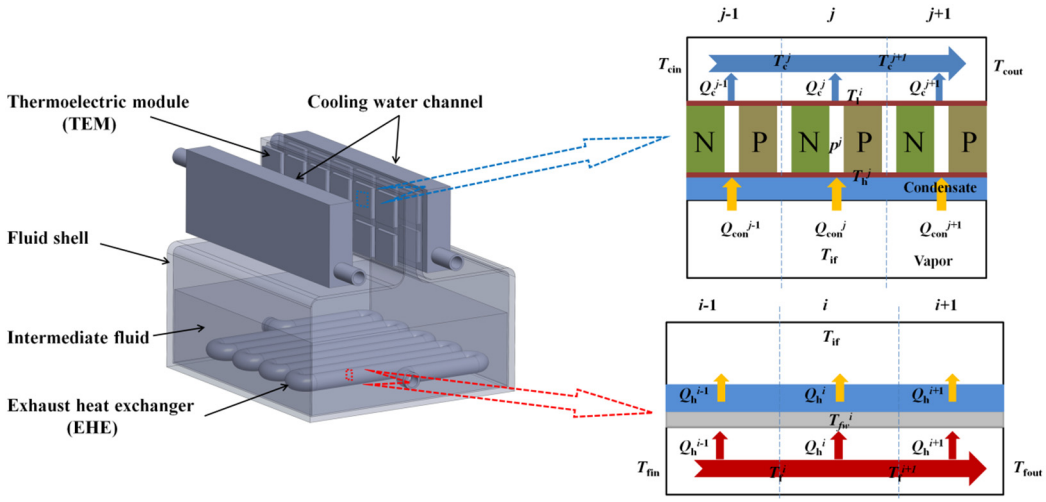

Figure 1. Intermediate fluid thermoelectric generator.

3. Mathematical Model

In the present study, a steady-state mathematical model of the IFTEG is established. To streamline the model, several aspects are neglected, including irradiation heat transfer and the lateral heat conduction of the EHE, the cooling water heat exchanger, and the cavity, which has little influence on the prediction of results [33]. It is assumed that the cavity contains no impurities apart from the IFD, thereby ensuring a gas–liquid phase equilibrium within the IFD. If impurities such as non-condensable gas are mixed into the cavity, it will cause the condensing heat transfer coefficient to decrease, thus lowering the temperature of the hot end of the module and reducing the power generation performance of the module. All TEMs are envisaged as being identically sized and connected in series. Contact thermal resistance and contact resistance at each interface are disregarded, and the Thomson effect is not taken into consideration [35].

As depicted in Figure 1, the entire IFTEG system can be segregated into two sections: the boiling section and the condensing section. In the boiling section, the surface area of the EHE is represented as S_{EHE}. The EHE is subdivided into n_{x} units, each possessing a surface area of A_{EHE}, along the direction of the exhaust flow. The ith exhaust heat transfer unit is selected for the analysis. The heat ${Q_{\mathrm{h}}}^{i}$, originating from the exhaust, instigates the boiling of the IFD, concurrently reducing the exhaust temperature from ${T_{\mathrm{f}}}^{i}$ to ${T_{\mathrm{f}}}^{i+1}$. Assuming the mean temperature of the exhaust inlet and outlet of the unit as the exhaust temperature and the temperature of the IFD as T_{if}, the energy equation of the boiling section control unit can be expressed as follows [34]:

$$Q_{\mathrm{h}}^{i} = m_{\mathrm{f}} c_{\mathrm{p,f}} (T_{\mathrm{f}}^{i} - T_{\mathrm{f}}^{i+1}) = (\frac{T_{\mathrm{f}}^{i} + T_{\mathrm{f}}^{i+1}}{2} - T_{\mathrm{if}}) / (\frac{1}{h_{\mathrm{f}} A_{\mathrm{EHE}}} + \frac{\delta_{\mathrm{EHE}}}{\lambda_{\mathrm{EHE}} A_{\mathrm{EHE}}} + \frac{1}{h_{\mathrm{e}} A_{\mathrm{EHE}}}) \quad (1)$$

In the above equation, m_{f}, $c_{\mathrm{p,f}}$, and h_{f} denote the mass flow, specific heat, and heat transfer coefficient of the exhaust, respectively. Meanwhile, δ_{EHE} and λ_{EHE} represent the thickness and thermal conductivity of the EHE, respectively. The boiling heat transfer coefficient of the IFD on the EHE surface is indicated by h_{e}, which can be calculated using Rohsenow's dimensionless correlation, and the physical properties of the IFD are calculated from the saturated temperature T_{if}.

The total heat exchange Q_{h} and area S_{EHE} across the entire boiling section can be expressed in the following manner:

$$Q_{\mathrm{h}} = \sum_{i=1}^{n_{\mathrm{x}}} Q_{\mathrm{h}}^{i} \quad (2)$$

Within the condensing section, the thermoelectric module (TEM) is distributed across two sides of the section. Given the perfect symmetry on both sides, a single-sided condensing section can be selected for analytical purposes. The complete condensing section encompasses $2n_y \times n_z$ TEMs, signifying that the number of modules on a single side is $n_y \times n_z$. Here, n_y denotes the number of TEMs distributed along the direction of the cooling water flow, while n_z represents the TEMs arranged in the vertical direction of the cooling water flow. In the cooling water flow direction, the thermoelectric performance of the module varies due to the gradual increase in cooling water temperature. However, the module performance is considered consistent in the vertical direction. Therefore, for the purposes of this analysis, the TEM in column j is selected as the research subject. The IFD condenses at the hot end of the TEM, with the released heat ($Q_{con}{}^j$) generating electricity (P^j) within the module. The residual heat ($Q_c{}^j$) is absorbed by the cooling water, leading to a rise in the cooling water temperature from $T_c{}^i$ to $T_c{}^{i+1}$. Consequently, the energy equation for the TEM in column j can be delineated as follows [34]:

$$Q_c^j = n_z\left[(\alpha_p - \alpha_n)IT_l^j + \frac{(\lambda_p + \lambda_n)lw}{z}(T_h^j - T_l^j) - 0.5I^2\frac{z(\rho_p + \rho_n)}{lw}\right] = (T_{if} - T_{cw})/(\frac{1}{n_z h_{con}^j F} + \frac{\delta_{shell}}{n_z F \lambda_{shell}}) \quad (3)$$

$$\begin{aligned} Q_c^j &= n_z\left[(\alpha_p - \alpha_n)IT_l^j + \frac{(\lambda_p+\lambda_n)lw}{z}(T_h^j - T_l^j) + 0.5I^2\frac{z(\rho_p+\rho_n)}{lw}\right] \\ &= (T_l^j - \frac{T_c^j + T_c^{j+1}}{2})/\left(\frac{1}{n_z F h_c} + \frac{\delta_{CHE}}{n_z F \lambda_{CHE}}\right) = c_{p,c} m_c (T_c^{j+1} - T_c^j) \end{aligned} \quad (4)$$

$$P^j = Q_{con}^i - Q_c^i \quad (5)$$

The parameters $\alpha_{p/n}$, $\lambda_{p/n}$, and $\rho_{p/n}$ denote the Seebeck coefficient, thermal conductivity, and resistivity of the P/N thermoelectric materials, respectively. The dimensions l, w, and z represent the length, width, and height of the P/N thermoelectric leg, respectively. F, δ_{CHE}, and λ_{CHE} correspond to the surface area, thickness, and thermal conductivity of the ceramic sheet, respectively. Meanwhile, δ_{shell} and λ_{shell} refer to the thickness and thermal conductivity of the cavity, respectively. I represents the current, while $T_h{}^j$ and $T_l{}^j$ symbolize the hot- and cold-end temperatures of the TEM, respectively. The condensation heat transfer coefficient of the IFD in the cavity h_{con} can be calculated in accordance with the Nusselt theory [34], and the physical properties of the IFD are calculated from the saturated temperature T_{if}. The parameters $c_{p,c}$, m_c, and h_c represent the specific heat, mass flow rate, and heat transfer coefficient of the cooling water, respectively.

The heat (Q_{con}) released by the IFD within the condensing section of the cavity can be formulated as follows:

$$Q_{con} = \sum_{j=1}^{n_y} Q_{con}^j \quad (6)$$

According to the conservation of energy, the heat absorbed and heat released in the cavity are the same when equilibrium is reached [35]:

$$Q_h = Q_{con} \quad (7)$$

Then, the TEM area, output power, and efficiency of the IFTEG can be expressed as:

$$S_{TEM} = 2n_x n_y F \quad (8)$$

$$P = \sum_{j=1}^{n_y} P^j \quad (9)$$

$$\eta = P/Q_h \times 100 \quad (10)$$

In the present study, water is selected as the IFD, and the principal boundary conditions are delineated in Table 1. The focus of this study is on the impact of exhaust parameters on the structural optimization of the IFTEG. The variation range of the exhaust parameters is established in accordance with the literature [35]. During the calculation process, an initial assumption is made for the temperature (T_{if}) of the IFD. Subsequently, the boiling heat transfer coefficient (h_e) and the condensation heat transfer coefficient (h_{con}) are calculated, factoring in the exhaust parameters and the cooling water parameters. This leads to the computation of the condensation heat transfer (Q_{con}) and the boiling heat transfer (Q_h). The temperature (T_{if}) is progressively corrected by ensuring the equivalence of Q_{con} and Q_h. Model validation, as previously articulated in the literature, will not be reiterated here [34].

Table 1. Main parameters of the system [27,29].

	Unit	Values
Exhaust temperature, T_{fin}	°C	250–550
Exhaust flow, m_f	g/s	5–55
Hot-side heat transfer coefficient, h_f	W/m^2K	80
Cooling water temperature, T_{cin}	°C	70
Cooling water flow, m_c	g/s	200
Cooling water heat transfer coefficient, h_c	W/m^2K	1000
Seebeck coefficient of P/N materials, $\alpha_{p/n}$	VK^{-1}	$2.037 \times 10^{-4}/-1.721 \times 10^{-4}$
Resistance of P/N materials, $\rho_{p/n}$	Ω·m	$1.314 \times 10^{-5}/1.119 \times 10^{-5}$
Thermal conductivity of P/N materials, $\lambda_{p/n}$	$Wm^{-1}K^{-1}$	1.265/1.011
Structure size of P-N leg, *l*/*w*/*z*	mm	5/5/5
Ceramic sheet size, *F*	mm^2	15×7.5

4. Results and Discussion

4.1. Effect of Exhaust Gas Parameters

In the present study, an initial examination of the thermoelectric characteristics of the novel generator is undertaken, with the findings illustrated in Figure 2. Given a constant EHE area (S_{EHE}), the output power displays an initial increase followed by a decrease with an increment in the TEM area (S_{TEM}), indicating the existence of an optimal TEM area ($S_{TEM,opt}$). This phenomenon can be attributed to the interplay between the exhaust heat exchange process in the boiling section and the thermoelectric conversion process within the module in the condensing section. As the S_{TEM} escalates, the condensation area within the chamber expands, enhancing the condensation heat transfer and leading to a reduction in the temperature of the IFD within the chamber. This temperature decrease elevates the heat transfer temperature differential between the liquid IFD and the exhaust, augmenting the boiling heat transfer, thereby resisting any further decline in the IFD temperature. Therefore, when a new equilibrium is established, the IFD temperature drops, which in turn reduces the hot-end temperature of the module and diminishes the thermoelectric performance of individual modules. The generator's overall output power is the cumulative total of all modules. Thus, under the combined influence of an increasing module number and a declining module generation performance, an optimal STEM ($S_{TEM,opt}$) exists to maximize the output power [34].

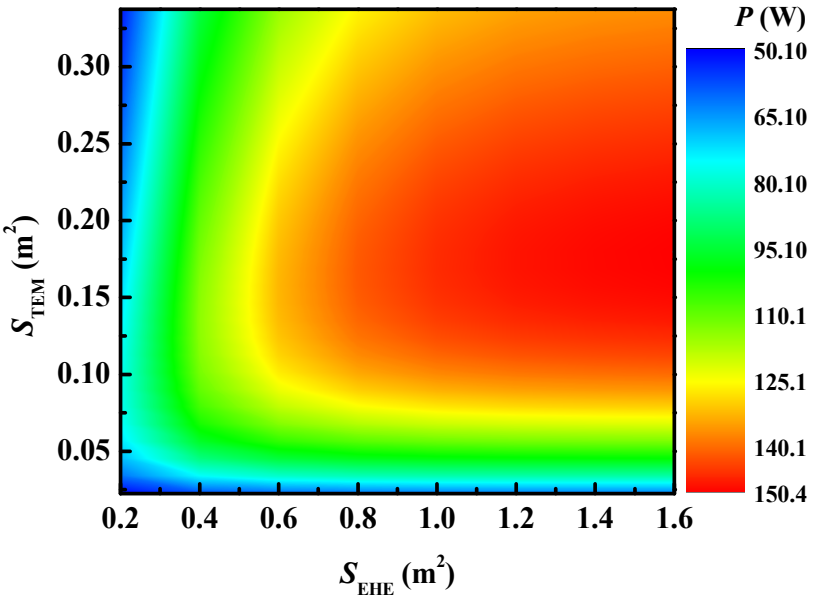

Figure 2. Effect of S_{TEM} and S_{EHE} on IFTEG performance (m_f = 20 g/s, T_{fin} = 350 °C).

As illustrated in Figure 2, the output power escalates progressively with an increase in the EHE area (S_{EHE}). This can be ascribed to the fact that an increment in S_{EHE} enhances the boiling heat transfer of the IFD, which in turn increases the IFD temperature within the chamber, leading to a rise in the output power. As the heat transfer capacity within the chamber increases, the area of the condensing section required to establish a new equilibrium also increases; consequently, $S_{TEM,opt}$ escalates. Furthermore, since the temperature of the IFD surpasses the exhaust outlet temperature, the performance improvement resulting from an increase in S_{EHE} gradually diminishes. Therefore, selecting an appropriate S_{EHE} is of paramount importance.

In real-world applications, exhaust parameters fluctuate in response to variations in vehicle operating conditions. Figure 3 further elucidates the influence of these exhaust parameters on the performance of the IFTEG. It can be observed that as both the exhaust temperature (T_{fin}) and flow rate (m_f) escalate, the maximum output power of the IFTEG incrementally increases. For instance, when T_{fin} equals 500 °C and m_f equals 50 g/s, the output power can reach an impressive 746 W. This can be attributed to the fact that an increase in either T_{fin} or m_f augments the boiling heat transfer, which subsequently raises the temperature of the IFD, leading to an increase in the hot-end temperature of the TEMs and thus enhancing the generation performance. Moreover, the optimal TEM area ($S_{TEM,opt}$) exhibits a significant increase with a rise in m_f, while the effect of T_{fin} on the optimal TEM area is comparatively minor. This indicates that maintaining optimal operating conditions for the IFTEG becomes challenging as exhaust parameters fluctuate, thereby complicating the optimization process of the IFTEG. Consequently, a pivotal issue to address in this study is how to design an efficient IFTEG that takes into account both exhaust parameters and the EHE area.

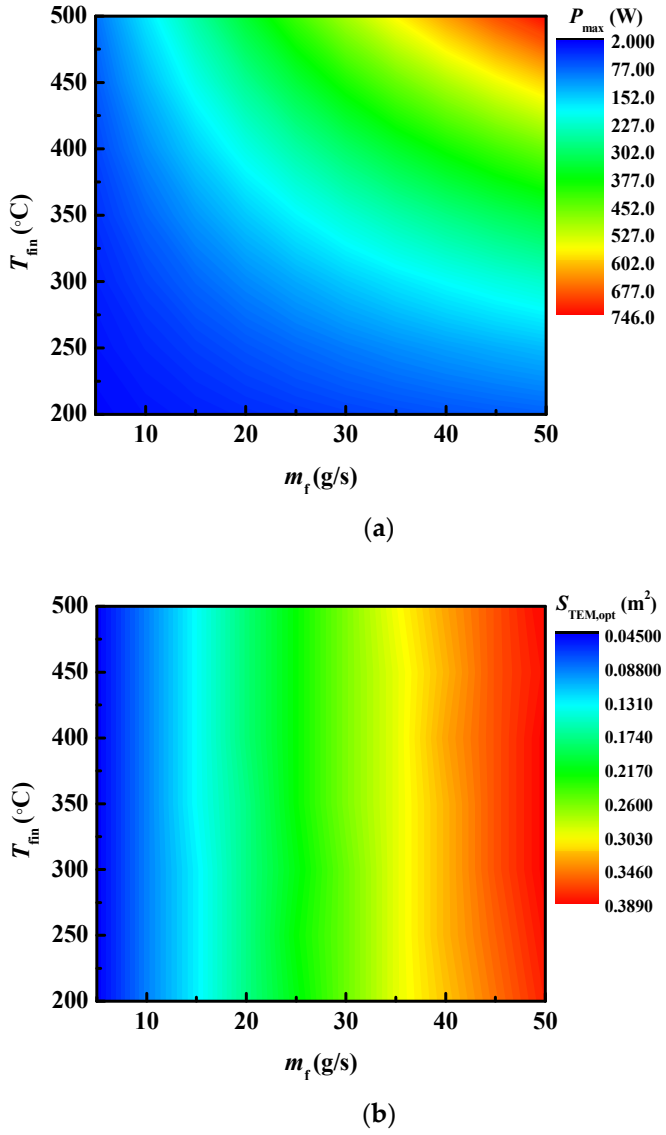

Figure 3. Effect of exhaust parameters (S_{EHE} = 1.6 m^2). (**a**) Maximum output power. (**b**) Optimal TEM area.

4.2. Optimal Design

The preceding analysis reveals that the optimal TEM area is influenced by the exhaust temperature, the flow, and the area of the EHE. Given that the range for the exhaust temperature, flow, and EHE area is predetermined, it is feasible to ascertain the $S_{TEM,opt}$ range. For instance, under the stipulated conditions, when the exhaust flow varies from 5 to 55 g/s, the exhaust temperature fluctuates between 250 and 550 °C, and the EHE area spans between 0.2 and 1.6 m^2, the optimal TEM area lies within the range of 0.042 to 0.383 m^2. Thus, during the generator's design phase, the designated thermoelectric module area ($S_{TEM,d}$) must fall within the range of 0.042 to 0.383 m^2.

In practical implementations, to assure adequate heat exchange between the exhaust and the IFD, thereby securing a larger power output, it is preferable to design an EHE area as large as permissible conditions allow. Therefore, in the subsequent analysis, S_{EHE} is assumed to be a constant value. Once S_{EHE} is set, the power output of the IFTEG becomes a function of the TEM area, exhaust flow, and exhaust temperature. When $S_{TEM,d}$ is fixed, the power output will fluctuate in response to changes in the exhaust temperature and flow. Given that $S_{TEM,d}$ cannot satisfy $S_{TEM,opt}$ under all exhaust flow or temperature conditions, the power output P ($S_{TEM,d}$, T_{fin}, m_f, S_{EHE}) of the system with the designed

TEM area $S_{TEM,d}$ must be lower than the maximum power output P_{max} ($S_{TEM,opt}$, T_{fin}, m_f, S_{EHE}) achieved when the system utilizes $S_{TEM,opt}$. This results in a deviation between the actual power output P and the maximum power output P_{max}. The power deviation is denoted as dev_d and defined as follows:

$$dev_d = \frac{P_{max}(S_{TEM,opt}, T_{fin}, m_f, S_{EHE}) - P(S_{TEM,d}, T_{fin}, m_f, S_{EHE})}{P_{max}(S_{TEM,opt}, T_{fin}, m_f, S_{EHE})} \times 100 \quad (11)$$

The aforementioned equation indicates that, as $S_{TEM,opt}$ is determined with the exhaust temperature (T_{fin}), the exhaust flow (m_f), and the area of the EHE (S_{EHE}), the power deviation is consequently a function of the designed thermoelectric module area ($S_{TEM,d}$), the exhaust temperature (T_{fin}), the exhaust flow (m_f), and the area of the EHE (S_{EHE}). The power deviation intensifies with an increasing disparity between the actual and maximum power outputs.

Upon the selection of $S_{TEM,d}$, a power deviation corresponds to each specific temperature and flow. Consequently, within the range of fluctuating flow and temperature, a peak power deviation is inevitably present. This can be expressed as:

$$\begin{cases} dev_{d,max} = \max\{dev_d\} \\ m_f \in \{5\ g/s, 55\ g/s\} \\ T_{fin} \in \{250\ °C, 550\ °C\} \end{cases} \quad (12)$$

In the quest for the optimally designed thermoelectric module area, a smaller peak power deviation is preferable. This implies that the selected thermoelectric module area can closely approximate the maximum power output under all operational conditions.

Figure 4 illustrates the relationship between power deviation and the designed TEM area ($S_{TEM,d}$) under varying exhaust flow conditions, given a constant EHE area (S_{EHE}) of 1.6 m^2 and an exhaust temperature (T_{fin}) of 350 °C. In scenarios where $S_{TEM,d}$ is relatively small, the power deviation escalates with an increasing exhaust flow. Conversely, with a larger $S_{TEM,d}$, the power deviation diminishes as the exhaust flow increases. The red line within the figure marks the evolution of peak power deviation against the differing $S_{TEM,d}$ under various flow conditions. The peak power deviation initially contracts and subsequently expands with the escalation in $S_{TEM,d}$. When $S_{TEM,d}$ is 0.135 m^2, the peak power deviation minimizes to 24.3%. This suggests that when SEHE is 1.6 m^2 and the exhaust temperature is 350 °C, the optimally designed thermoelectric module area ($S_{TEM,d,opt}$) is 0.135 m^2. This configuration ensures that the power output deviation from the system, within the exhaust flow range of 5 to 55 g/s, remains less than 24.3% from the maximum power output.

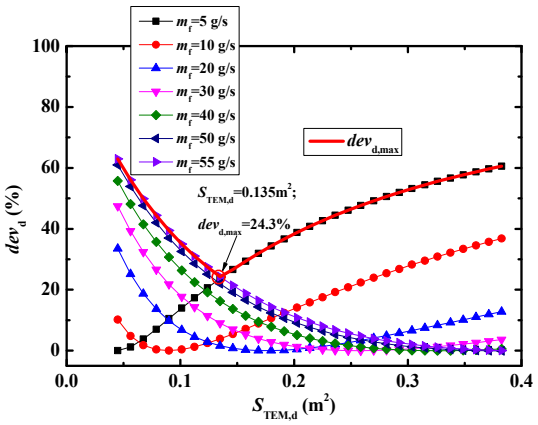

Figure 4. Variation in power deviation with $S_{TEM,d}$ under different exhaust flow conditions (S_{EHE} = 1.6 m^2, T_{fin} = 350 °C).

Figure 5 demonstrates the variation in power deviation with the designed TEM area ($S_{TEM,d}$) at distinct exhaust temperatures, given a constant EHE area (S_{EHE}) of 1.6 m^2 and an exhaust flow rate of 10 g/s. As $S_{TEM,d}$ is reduced, the power deviation gradually increases with the rise in exhaust temperature, whereas an inverse pattern is observed when $S_{TEM,d}$ is substantial. This trend mirrors the changes observed in relation to the exhaust flow rate. Nevertheless, the overall impact of exhaust temperature on power deviation is relatively minor.

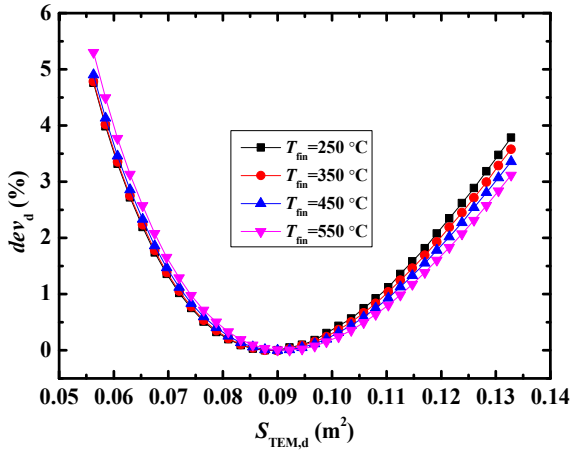

Figure 5. Variation in power deviation with $S_{TEM,d}$ at different exhaust temperatures (S_{EHE} = 1.6 m^2, m_f = 10 g/s).

From the preceding analysis, it is discerned that for a fixed S_{EHE}, regardless of the $S_{TEM,d}$ chosen, the power deviation will fluctuate in response to changes in the exhaust temperature and flow rate, but within certain constraints. Consequently, a peak power deviation materializes. Figure 6 delineates the variation of the peak power deviation of the IFTEG in relation to $S_{TEM,d}$. As $S_{TEM,d}$ enlarges, the peak power deviation initially contracts and subsequently expands. An optimal $S_{TEM,d}$ of 0.124 m^2 minimizes the peak power deviation to 27.5%. Hence, when designing the IFTEG with a S_{EHE} of 1.6 m^2, the optimal $S_{TEM,d}$ should be set at 0.124 m^2.

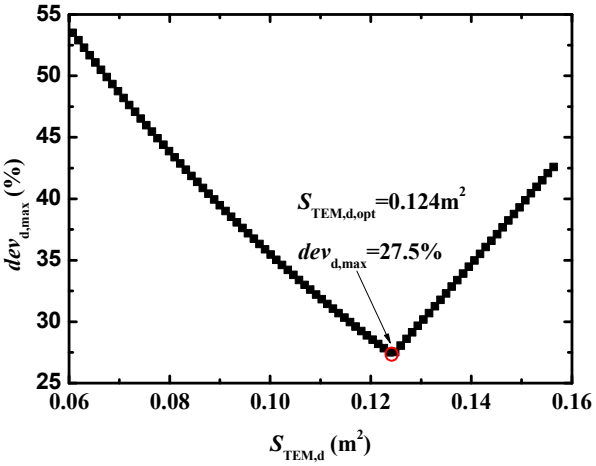

Figure 6. Variation in peak power deviation with $S_{TEM,d}$ (S_{EHE} = 1.6 m^2).

As previously discussed, the area of the exhaust heat exchanger (S_{EHE}) plays a pivotal role in the design of the novel thermoelectric generator. The preceding analysis was conducted assuming S_{EHE} to be constant. Despite a larger area being desirable in the design process, practical constraints such as exhaust channel installation limits may preclude

the fabrication of a sufficiently expansive EHE. Thus, it becomes essential to analyze the impact of S_{EHE} on the optimal design of the thermoelectric module area ($S_{TEM,d,opt}$). Figure 7 illustrates the variation in $S_{TEM,d,opt}$ as a function of S_{EHE}. As the area of the EHE escalates, the optimally designed TEM area incrementally expands, although the extent of this increase progressively diminishes. Moreover, the following fitting formula for the optimal $S_{TEM,d,opt}$ can assist in the design of the IFTEG:

$$S_{TEM,d,opt} = 0.12498 - 0.09031 * 0.97199^{h_f S_{EHE}} \quad (13)$$

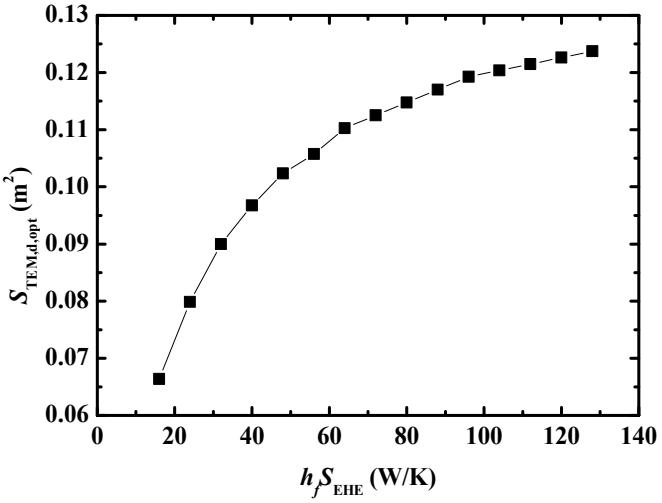

Figure 7. Variation in the $S_{TEM,d}$ with S_{EHE}.

5. Conclusions

The intermediate fluid thermoelectric generator (IFTEG) has demonstrated remarkable efficiency in harnessing waste heat from exhaust gases for power generation. Nevertheless, its intricate structure and the variable nature of operating parameters complicate the design process. This study employed the peak power deviation approach to optimize this novel system and determine the ideal design parameters. The key conclusions drawn from the results are as follows:

(1) Within the IFTEG system, an optimal thermoelectric module (TEM) area exists that maximizes output power. Both the maximum output power and the optimal TEM area progressively increase with the enlargement of the exhaust heat exchanger (EHE) area.

(2) As the exhaust temperature ascends, the maximum output power exhibits a corresponding rise, whereas the optimal TEM area remains relatively stable. Conversely, an increase in the exhaust flow rate amplifies both the maximum output power and the optimal TEM area.

(3) The peak power deviation methodology is proposed to ascertain the optimal TEM area for design. A smaller peak power deviation implies that the designed TEM area is in closer alignment with the optimal TEM area.

(4) As the designed TEM area expands, the peak power deviation initially reduces before experiencing an upswing. An optimally designed TEM area exists, corresponding to a minimum value, which allows the exhaust operation to approach the best working conditions within a certain range as closely as possible. A 1.6 m^2 EHE area yields an optimally designed TEM area of 0.124 m^2. As the EHE area grows, the optimally designed TEM area is expected to follow a similar trend.

Author Contributions: W.Z.: Methodology, Writing—original draft. W.L.: Software, Data curation. S.L.: Writing—review and editing. L.X.: Software. M.G.: Conceptualization, Writing—review and editing. Y.Z.: Supervision, Writing—review and editing. All authors have read and agreed to the published version of the manuscript.

Funding: This research was funded by Natural Science Foundation of China (51906056), National Key Research and Development Program of China (2022YFE0019100), Open Project Program of the Hebei Technology Innovation Center of Phase Change Thermal Management of Data Center (SKF-2022-3), and Hebei Natural Science Foundation (E2020412176).

Data Availability Statement: The date presented in this study are available on request from the corresponding author.

Acknowledgments: The authors are grateful to the Natural Science Foundation of China (51906056), National Key Research and Development Program of China (2022YFE0019100), Open Project Program of the Hebei Technology Innovation Center of Phase Change Thermal Management of Data Center (SKF-2022-3), and Hebei Natural Science Foundation (E2020412176).

Conflicts of Interest: There are no conflict of interest to declare.

References

1. Oluleye, G.; Smith, R.; Jobson, M. Modelling and screening heat pump options for the exploitation of low grade waste heat in process sites. *Appl. Energy* **2016**, *169*, 267–286. [CrossRef]
2. Twaha, S.; Zhu, J.; Yan, Y.; Li, B. A comprehensive review of thermoelectric technology: Materials, applications, modelling and performance improvement. *Renew. Sustain. Energy Rev.* **2016**, *65*, 698–726. [CrossRef]
3. Wang, Y.; Xu, H.; He, W.; Zhao, Y.; Wang, X. Lattice Boltzmann simulation of the structural degradation of a gas diffusion layer for a proton exchange membrane fuel cell. *J. Power Sources* **2023**, *556*, 232452. [CrossRef]
4. Nonthakarn, P.; Ekpanyapong, M.; Nontakaew, U.; Bohez, E. Design and Optimization of an Integrated Turbo-Generator and Thermoelectric Generator for Vehicle Exhaust Electrical Energy Recovery. *Energies* **2019**, *12*, 3134. [CrossRef]
5. Zhao, Y.; Lu, M.; Li, Y.; Wang, Y.; Ge, M. Numerical investigation of an exhaust thermoelectric generator with a perforated plate. *Energy* **2023**, *263*, 125776. [CrossRef]
6. Chen, W.; Wu, P.; Lin, Y. Performance optimization of thermoelectric generators designed by multi-objective genetic algorithm. *Appl. Energy* **2018**, *209*, 211–223. [CrossRef]
7. Luo, D.; Yan, Y.; Chen, W.-H.; Yang, X.; Chen, H.; Cao, B.; Zhao, Y. A comprehensive hybrid transient CFD-thermal resistance model for automobile thermoelectric generators. *Int. J. Heat Mass Transf.* **2023**, *211*, 124203. [CrossRef]
8. Kempf, N.; Zhang, Y. Design and optimization of automotive thermoelectric generators for maximum fuel efficiency improvement. *Energy Convers. Manag.* **2016**, *121*, 224–231. [CrossRef]
9. Zhao, Y.; Lu, M.; Li, Y.; Ge, M.; Xie, L.; Liu, L. Characteristics analysis of an exhaust thermoelectric generator system with heat transfer fluid circulation. *Appl. Energy* **2021**, *304*, 117896. [CrossRef]
10. Lu, X.; Yu, X.; Qu, Z.; Wang, Q.; Ma, T. Experimental investigation on thermoelectric generator with non-uniform hot-side heat exchanger for waste heat recovery. *Energy Convers. Manag.* **2017**, *150*, 403–414. [CrossRef]
11. Ma, T.; Lu, X.; Pandit, J.; Ekkad, S.V.; Huxtable, S.T.; Deshpande, S.; Wang, Q. Numerical study on thermoelectric–hydraulic performance of a thermoelectric power generator with a plate-fin heat exchanger with longitudinal vortex generators. *Appl. Energy* **2017**, *185*, 1343–1354. [CrossRef]
12. Chen, W.; Wang, C.; Huat, L.; Hoang, A.T.; Bandala, A.A. Performance evaluation and improvement of thermoelectric generators (TEG): Fin installation and compromise optimization. *Energy Convers. Manag.* **2021**, *250*, 114858. [CrossRef]
13. Marvão, A.; Coelho, P.J.; Rodrigues, H.C. Optimization of a thermoelectric generator for heavy-duty vehicles. *Energy Convers. Manag.* **2019**, *179*, 178–191. [CrossRef]
14. Luo, D.; Sun, Z.; Wang, R. Performance investigation of a thermoelectric generator system applied in automobile exhaust waste heat recovery. *Energy* **2022**, *238*, 121816. [CrossRef]
15. Liu, C.; Deng, Y.; Wang, X.; Liu, X.; Wang, Y.; Su, C. Multi-objective optimization of heat exchanger in an automotive exhaust thermoelectric generator. *Appl. Therm. Eng.* **2016**, *108*, 916–926. [CrossRef]
16. Fernández-Yañez, P.; Armas, O.; Capetillo, A.; Martínez-Martínez, S. Thermal analysis of a thermoelectric generator for light-duty diesel engines. *Appl. Energy* **2018**, *226*, 690–702. [CrossRef]
17. Su, C.; Wang, W.; Liu, X.; Deng, Y. Simulation and experimental study on thermal optimization of the heat exchanger for automotive exhaust-based thermoelectric generators. *Case Stud. Therm. Eng.* **2014**, *4*, 85–91. [CrossRef]
18. Su, C.; Huang, C.; Deng, Y.; Wang, Y.; Chu, P.; Zheng, S. Simulation and Optimization of the Heat Exchanger for Automotive Exhaust-Based Thermoelectric Generators. *J. Electron. Mater.* **2015**, *45*, 1464–1472. [CrossRef]
19. Karana, D.R.; Sahoo, R.R. Performance assessment of the automotive heat exchanger with twisted tape for thermoelectric based waste heat recovery. *J. Clean. Prod.* **2021**, *283*, 124631. [CrossRef]

20. Lesage, F.J.; Sempels, É.V.; Lalande-Bertrand, N. A study on heat transfer enhancement using flow channel inserts for thermoelectric power generation. *Energy Convers. Manag.* **2013**, *75*, 532–541. [CrossRef]
21. Wang, Y.; Li, S.; Zhang, Y.; Yang, X.; Deng, Y.; Su, C. The influence of inner topology of exhaust heat exchanger and thermoelectric module distribution on the performance of automotive thermoelectric generator. *Energy Convers. Manag.* **2016**, *126*, 266–277. [CrossRef]
22. Wang, Y.; Li, S.; Xie, X.; Deng, Y.; Liu, X.; Su, C. Performance evaluation of an automotive thermoelectric generator with inserted fins or dimpled-surface hot heat exchanger. *Appl. Energy* **2018**, *218*, 391–401. [CrossRef]
23. Choi, Y.; Negash, A.; Kim, T.Y. Waste heat recovery of diesel engine using porous medium-assisted thermoelectric generator equipped with customized thermoelectric modules. *Energy Convers. Manag.* **2019**, *197*, 111902. [CrossRef]
24. Negash, A.A.; Choi, Y.; Kim, T.Y. Experimental investigation of optimal location of flow straightener from the aspects of power output and pressure drop characteristics of a thermoelectric generator. *Energy* **2021**, *219*, 119565. [CrossRef]
25. Li, Y.; Wang, S.; Zhao, Y.; Lu, C. Experimental study on the influence of porous foam metal filled in the core flow region on the performance of thermoelectric generators. *Appl. Energy* **2017**, *207*, 634–642. [CrossRef]
26. Bai, W.; Yuan, X.; Liu, X. Numerical investigation on the performances of automotive thermoelectric generator employing metal foam. *Appl. Therm. Eng.* **2017**, *124*, 178–184. [CrossRef]
27. Musial, M.; Borcuch, M.; Wojciechowski, K. The Influence of a Dispersion Cone on the Temperature Distribution in the Heat Exchanger of a Thermoelectric Generator. *J. Electron. Mater.* **2015**, *45*, 1517–1522. [CrossRef]
28. Shu, G.; Ma, X.; Tian, H.; Yang, H.; Chen, T.; Li, X. Configuration optimization of the segmented modules in an exhaust-based thermoelectric generator for engine waste heat recovery. *Energy* **2018**, *160*, 612–624. [CrossRef]
29. Shen, Z.; Huang, B.; Liu, X. Effect of structure parameters on the performance of an annular thermoelectric generator for automobile exhaust heat recovery. *Energy Convers. Manag.* **2022**, *256*, 115381. [CrossRef]
30. Luo, D.; Liu, Z.; Yan, Y.; Li, Y.; Wang, R.; Zhang, L.; Yang, X. Recent advances in modeling and simulation of thermoelectric power generation. *Energy Convers. Manag.* **2022**, *273*, 116389. [CrossRef]
31. Aranguren, P.; Araiz, M.; Astrain, D.; Martínez, A. Thermoelectric generators for waste heat harvesting: A computational and experimental approach. *Energy Convers. Manag.* **2017**, *148*, 680–691. [CrossRef]
32. Garud, K.S.; Seo, J.H.; Patil, M.S.; Bang, Y.M.; Pyo, Y.D.; Cho, C.P.; Lee, M.Y. Thermal–electrical–structural performances of hot heat exchanger with different internal fins of thermoelectric generator for low power generation application. *J. Therm. Anal. Calorim.* **2020**, *143*, 387–419. [CrossRef]
33. He, H.; Wu, Y.; Liu, W.; Rong, M.; Fang, Z.; Tang, X. Comprehensive modeling for geometric optimization of a thermoelectric generator module. *Energy Convers. Manag.* **2019**, *183*, 645–659. [CrossRef]
34. Zhao, Y.; Wang, S.; Ge, M.; Liang, Z.; Liang, Y.; Li, Y. Performance investigation of an intermediate fluid thermoelectric generator for automobile exhaust waste heat recovery. *Appl. Energy* **2019**, *239*, 425–433. [CrossRef]
35. Ge, M.; Li, Z.; Zhao, Y.; Xie, L.; Wang, S. Effect of exhaust parameters on performance of intermediate fluid thermoelectric generator. *Case Stud. Therm. Eng.* **2021**, *28*, 101480. [CrossRef]

Disclaimer/Publisher's Note: The statements, opinions and data contained in all publications are solely those of the individual author(s) and contributor(s) and not of MDPI and/or the editor(s). MDPI and/or the editor(s) disclaim responsibility for any injury to people or property resulting from any ideas, methods, instructions or products referred to in the content.